Soft Matter

RSC Publishing

PAPER

View Article Online
View Journal

Flow-controlled densification and anomalous dispersion of *E. coli* through a constriction†

Cite this: DOI: 10.1039/c2sm26460a

E. Altshuler,[abc] G. Miño,[a] C. Pérez-Penichet,[b] L. del Río,[b] A. Lindner,[a] A. Rousselet[a] and E. Clément*[a]

Dispersion and migration of bacteria under flow in tortuous and confined structures such as porous or fractured materials is related to a large spectrum of practical interest, but is still poorly understood. Here, we address the question of transport and dispersion of an *E. coli* suspension flowing through a micro-fluidic channel with a funnel-like constriction in its center. We show a counter-intuitive symmetry breaking of the bacterial concentration, which increases significantly past the funnel. This concentration enhancement persists over large distances from the funnel and disappears at large flow rate values. We map our results onto a one dimensional convection–diffusion equation predicting quantitatively the experimental results, without free parameters, when a conservative non-local source term is introduced. This last term, measured experimentally, represents a long range memory effect due to the unbalance of wall adsorption and desorption processes past the constriction. Our model experiment points out the generic importance of considering such constriction effects in the description of transport properties of active matter in porous media. It also opens the possibility to control the concentration of bacterial suspensions in micro-fluidic channels by simply tuning the flow intensity or direction.

Received 23rd June 2012
Accepted 21st November 2012

DOI: 10.1039/c2sm26460a

www.rsc.org/softmatter

From the hydrodynamics point of view, assemblies of microscopic swimmers such as bacteria dispersed in a fluid display constitutive properties differing strongly from those of passive suspensions.[1–3] Momentum transport equations and constitutive relationships are deeply modified by the presence of these autonomous swimmers dispersed in the fluid. New and surprising effects were reported such as activated Brownian motion,[4–6] anomalous viscosity,[7,8] mixing enhancement,[9] bio-convection[10] or work extraction from fluctuations.[11] Along those lines, the fundamental question of hydrodynamic dispersion of bacteria suspended in a fluid remains an issue that has not yet received a fully satisfactory treatment. This difficult question is closely linked to many practical issues related to bio-contamination in porous rocks, in biological micro-vessels or through medical catheters. Methods of analysis used to describe bacterial transport consist essentially of macroscopic convection–diffusion equations in association with adsorption–desorption terms describing retention effects by the surfaces. However, in spite of the fact that many fitting parameters can be used to match the dispersion curves, systematic inconsistencies were reported between experiment and modeling[12] and may lead to further phenomenological refinements including, for example, straining effect as in the colloidal filtration problem which would occur at the smallest pores and at the grain–grain junction.[13] Consequently, there is a strong and timely need to identify precisely the many processes at work contributing to the transport of bacteria in a confined environment, including those directly related to the micro-organism swimming capability.

In this work we will use suspensions of *E. coli*, a micro-organism that can move at low Reynolds number in aqueous media at a speed of about 20 microns per second. The *E. coli* mode of propulsion is rather well understood.[14] This 2 μm body-length swimmer produces a thrust due to the counter-clockwise rotation of a helical bundle of 10 μm length flagella. In the bulk, for the wild-type strain, the motion is made of straight "runs" interrupted every few seconds by a sudden change of direction (or "tumble").[15] The tumbling rate is triggered by chemotaxy *i.e.* complex intracellular biochemical cascades triggering the flagella rotation relative to fine strategies for finding nutriments.[16] In the vicinity of a solid boundary, the swimming picture drastically changes.[17–19] Lubrication forces acting on the counter-rotating body lead generically to circular trajectories. Experimental measurements and hydrodynamic studies suggest that solid boundaries also act as "traps".[20] The bacteria stay at the surface for a long time and this persistent motion induces a strong increase of concentration at the walls.[21] The recent use of microfluidic tools has revolutionized the way the

[a]PMMH, UMR 7636 CNRS-ESPCI-Universités Pierre et Marie Curie and Denis Diderot, 10, rue Vauquelin, 75231 Paris Cedex 5, France. E-mail: eric.clement@espci.fr
[b]"Henri Poincaré" Group of Complex Systems and Superconductivity Laboratory, Physics Faculty-IMRE, University of Havana, 10400 Havana, Cuba
[c]Centre for Advanced Study, Norwegian Academy of Sciences and Letters, NO-0271, Oslo, Norway

† Electronic supplementary information (ESI) available. See DOI: 10.1039/c2sm26460a

microorganisms motility can be approached experimentally. The fabrication of microscopic scale channels of different forms, enabling observations of high spatial and temporal resolution, allows crucial tests of many fundamental hypotheses on transport properties. Furthermore, such channels can directly be used to enhance the selection of target species depending on their motile character. For bacterial suspensions such tools have recently been used to describe spontaneous densification induced by wall shape asymmetry,[22,23] upstream trajectories in the presence of flow[24] or chemotactic response in well controlled chemical gradients.[25]

In the present work, we will use microfluidic channels to visualize the effect of a funnel like constriction on the bacterial transport in a flow. This geometry can be seen as a situation encountered generically in many porous structures at the pore necks. For appropriate flow conditions, a strong concentration enhancement of active bacteria is observed past the funnel, opposite to observations for complex flows containing "inactive" particles.[26] Our main aim in this paper is to describe this novel and counter intuitive phenomenon. We discuss our results in the light of elementary mechanisms of interaction between the swimming bacteria and the walls. To render quantitatively the dispersion curves, we propose an advection–diffusion equation containing an effective long range source term that is directly related to the specific swimming properties of the bacteria at the walls.

1 Experimental set-up

The bacterial suspension is a wild-type strain of *E. coli* W (ATCC 11105 (ref. 27)) prepared in a "minimal motility medium", as follows. Wild type *E. coli* W, ATCC 11105 were grown overnight in a rich culture medium (LB). From this sample 40 μL of bacteria were diluted in 8 mL of LB. They were incubated for at least five hours to obtain a maximal activity.[28] After washing, they were transferred into Minimal Motility Media MMA[29] (10 mM NaH_2PO_4, 10 mM K_2HPO_4, 0.1 mM EDTA, and 20 mM sodium lactate), supplemented with K-acetate (0.34 mM) and polyvinyl pyrolidone (PVP: 0.005%). The overall concentration of bacteria was kept at $4 \pm 0.5 \times 10^8$ bact. per mL. We checked that the suspending fluid was Newtonian (viscosity $\eta = 0.88$ mPa s at 25 °C). All experiments were performed at a fixed temperature $T = 25$ °C. The minimal motility medium is a controlled environment where bacteria can swim but do not replicate and where the influence of chemotaxis or aerotaxis driving the bacterial motion is limited. We also use, for comparison, suspensions of dead-bacteria obtained under identical conditions but killed using ethanol at 80%.

Note that at the small concentrations we use, the suspensions can be considered to be in the dilute regime where interactions between bacteria can be neglected and the viscosity of the suspension is not different from the viscosity of the suspending fluid.

The bacterial suspension is flowed by gravity overpressure through a microfluidic channel of total length $L = 15$ mm made in PDMS by a standard soft-lithography technique (see Fig. 1(a)). The channels were fabricated onto glass covered by a 28 μm-thick PDMS coating to avoid sticking of the bacteria. The inlet and the outlet are inox tubes of 1 mm outer diameter connected to flexible plastic tubes. The rectangular section has a width $W = 200$ μm and a depth $h = 20$ μm and the channel contains, in its middle, a symmetric constriction over a distance $L_f = 200$ μm and reaches a minimum width $W_f = 40$ μm (see Fig. 1(a)). In Fig. 1(b), we show a bottom view of the channel in the vicinity of the constriction. Under our flow conditions the Reynolds number $\mathrm{Re} = \rho VL/\eta$, with ρ being the density, L a typical length scale and V a typical velocity, is found to be below 10^{-2}.

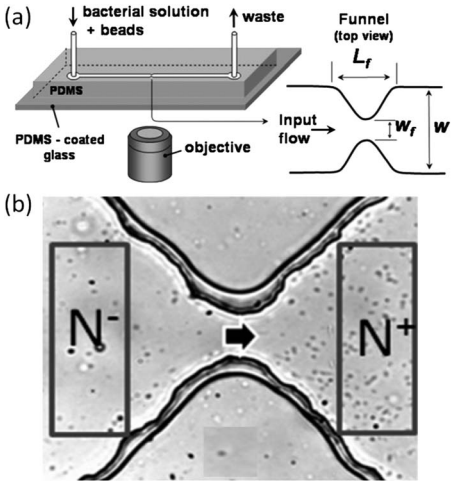

Fig. 1 (a) Sketch of the microfluidic channel fixed on a glass plate. On the right side, zoom on the funnel geometry viewed from the top; the dimensions are $L_f = 200$ μm, $W_f = 40$ μm and $W = 200$ μm (b). Visualization of the symmetry breaking effect at the funnel for an active *E. coli* suspension for $\langle V_x \rangle = 25$ μm s^{-1}. Display of the two symmetric rectangular domains where the number of bacteria N^- and N^+ is computed. The thick arrow corresponds to the flow direction.

The flowing suspensions were observed from below using an inverted microscope (Zeiss-Observer, Z1-magnification 40× or 20×). A digital camera PixeLINK PL-A741-E was used for image acquisition, (600 × 800 pix^2 and 1280 × 1024 pix^2) capturing videos at a frame rate of 20 and 12.5 frame/s, depending if the magnification used was 40× or 20×. Due to the relatively small height of the channel, all bacteria could be visualized along the vertical axis at a fixed position of the objective lens. For counting bacteria, the background of each video was digitally homogenized and "binarized" with appropriate thresholds to reveal all the individuals.

As can be seen in the snapshot shown in Fig. 1(b), at the junction between the lateral walls and the top and bottom surface there is a small apparent bulge. The lateral wall is straight over most of the channel height. However, the bulge at the junction corner makes the visualization of the bacterial motion very close to the *lateral* walls (typically at a 5 μm distance) difficult. These bacteria will not be considered in the first part of the paper and their role will be discussed later.

The base flow in our microfluidic channel is described by the classical results for flow at low Reynolds numbers in square channels.[30] The ratio between the average velocity far away from the constriction and the average velocity inside the constriction

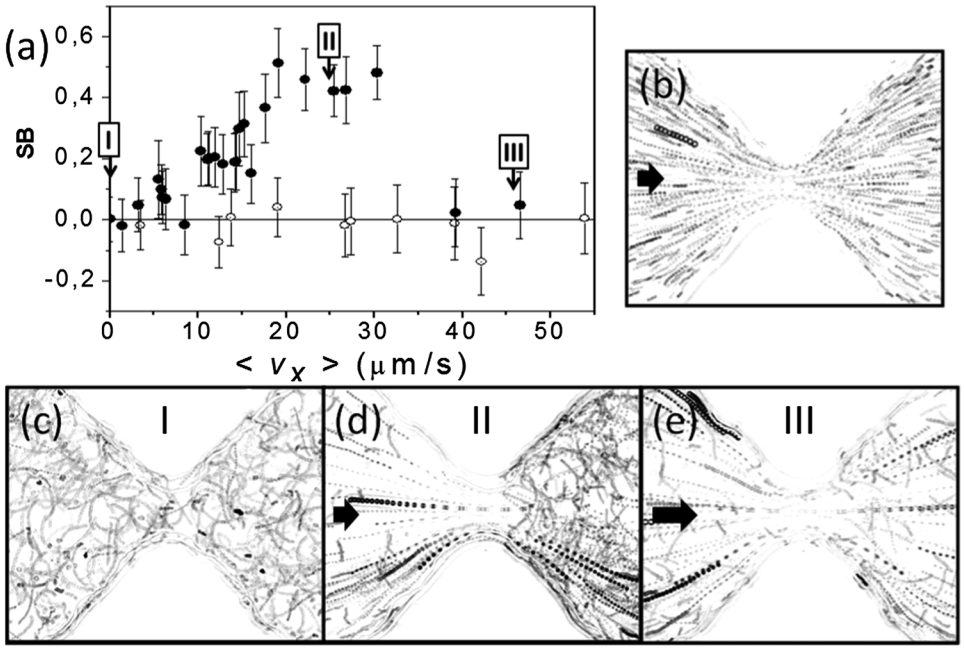

Fig. 2 Flow-controlled symmetry breaking in the concentration of *E. coli*. (a) SB as a function of the mean flow velocity $\langle V_x \rangle$. Error bars correspond to RMS fluctuations. Dark symbols are for living bacteria and empty symbols are for dead bacteria. Trajectories obtained by snapshot accumulation over 1 s (20 frames) for (b) dead bacteria at $\langle V_x \rangle = 25\ \mu m\ s^{-1}$ and for live bacteria at three mean flow velocities (c) $\langle V_x \rangle = 0\ \mu m\ s^{-1}$, (d) $\langle V_x \rangle = 25\ \mu m\ s^{-1}$ and (e) $\langle V_x \rangle = 45\ \mu m\ s^{-1}$. The corresponding roman numbers I, II, and III are displayed in (a). Note that trajectories corresponding to the beads appear as bigger circular spots in (b), (d) and (e). Flow is from left to right as indicated by the arrows.

is given by flux conservation to be W_f/W. Streamlines averaged over the height of the channel can be seen in Fig. 2(b), showing the trajectories of dead bacteria acting as passive tracer particles. As expected for low Reynolds number flows, the streamlines are found to be symmetrical with respect to both the transverse and the longitudinal axes. Note however that the flow directly upstream of the constriction is convergent in the flow direction, whereas the flow directly downstream is divergent.

Polystyrene beads of diameter $d = 2\ \mu m$ were dispersed in the suspension to serve as flow tracers. For a given overpressure, the average flow velocity $\langle V_x \rangle$ was estimated by averaging the tracer velocities detected in the constriction and multiplying its value by the ratio W_f/W. In principle, if one assumes a random distribution of passive tracers in the flow, this measurement provides a reasonable estimation of the mean flow velocity.

2 Flow induced symmetry breaking

We use bacterial suspensions prepared with a concentration $n = 4 \pm 0.5 \times 10^8$ bact. per mL. Fig. 1(b) displays a snapshot obtained at a mean flow velocity $V = 25\ \mu m\ s^{-1}$ where an accumulation of bacteria is clearly observed at the right side of the funnel. To quantify this effect the bacteria were counted inside two rectangular regions placed symmetrically on both sides of the funnel: N^- on the left and N^+ on the right (counting was done over 20 s with an acquisition frequency of 20 frames per s). We quantify the difference in bacterial concentration on both sides of the funnel by defining a symmetry breaking parameter:

$$\mathrm{SB} = \frac{N^+ - N^-}{N^+ + N^-} \quad (1)$$

In Fig. 2(a), we display SB as a function of the mean flow velocity $\langle V_x \rangle$ both for living and dead bacteria. In the case of living bacteria, starting from zero flow, the symmetry breaking parameter increases roughly linearly up to approximately SB = 0.6 as the mean flow velocity increases from zero to 20 $\mu m\ s^{-1}$. SB starts to differ from 0 at mean flow velocities of around 10 $\mu m\ s^{-1}$, corresponding to a maximal shear rate at the side walls of about 30 s^{-1}. SB then reaches a plateau and finally decays to zero quite abruptly around a mean flow velocity 40 $\mu m\ s^{-1}$. Note that SB reaches its maximum value at a velocity around 20–30 $\mu m\ s^{-1}$, a value comparable to the mean bacterial velocity measured in the absence of flow ($V_b = 15 \pm 5\ \mu m\ s^{-1}$). For suspensions of dead bacteria, the amount of individuals in the control regions before and after the constriction was identical, regardless of the flow velocity (see Fig. 2(a), hollow circles). This shows that the symmetry breaking effect is directly related to the active character of the suspension. In Fig. 2(c)–(e), we show that the symmetry breaking is also associated with a change in the trajectory shapes. In these figures, we display the tracks of bacteria and tracer particles obtained by superimposing snapshots acquired over 1 *s* (20 frames). At zero flow (Fig. 2(c)), the trajectory shapes are clearly curved and mostly circular which is a signature that on both sides of the funnel the bacteria dwell preferentially at the top/bottom wall. The situation changes drastically when the symmetry breaking is established. In Fig. 2(d), corresponding to the symmetry breaking plateau ($\langle V_x \rangle = 25\ \mu m\ s^{-1}$), one can clearly observe asymmetry in the

trajectory shapes before and after the funnel. Before the funnel, bacteria are convected mostly passively by the flow with trajectories identical to the latex particles appearing as thick tracks in the figures. However, past the funnel, the bacterial trajectories are much more curved, showing a net tendency to swim very close to the upper and lower boundaries. Finally, at high speeds ($\langle V_x \rangle = 45$ μm s^{-1}), most trajectories follow the streamlines as passive particles do (see Fig. 2(e)).

The symmetry breaking of the concentration profile can be controlled by changing not only the intensity, but the *direction* of the imposed flux. For example, starting with a flux of $\langle V_x \rangle = 25$ μm s^{-1} from left to right, we get a symmetry breaking parameter SB ≈ 0.6 (higher concentration of bacteria at the right of the funnel). If we then reverse the direction of the flow to $\langle V_x \rangle = -25$ μm s^{-1}, a value SB ≈ −0.6 is (*i.e.*, the higher concentration has moved to the left of the funnel; see VideoS1 and Fig. S1 in the ESI†). The process typically takes 10 s to reverse the flow and another 10–20 s to reach steady state and can be repeated several times with no obvious memory effects.

Next, we study the spatial range of concentration increase induced by the symmetry breaking. After establishing a constant flux of 30 μm s^{-1} for a few minutes, we performed a series of 14 spatially overlapping videos spanning a 5000 μm range along the channel, symmetrical around the constriction. Each video was taken at a 20× magnification and lasted 8 seconds (taken at 12.5 frames per s). From these movies, the time averaged bacterial density $n(x)$ along the flow was computed (the stripe width used for density measurements was $\Delta x = 5$ μm). In Fig. 3, we display the density profile $n(x)$. Before the funnel, the concentration is constant, around 5×10^8 bact. per mL and suddenly decreases to less than 1×10^8 bact. per mL at approximately −150 μm left from the geometrical center of the funnel. Then, a sharp increase in concentration occurs at the center of the funnel, reaching 14×10^8 bact. per mL at approximately 70 μm from the funnel center. This measurement shows not only the huge concentration amplification resulting from the flow constriction but also the long-range effect since the bacterial densification persists several millimeters past the funnel *i.e.* a distance larger by one order of magnitude than the funnel length L_f. Note that at a distance of 2.5 mm to the right of the funnel, the average concentration is still slightly higher than its value at the left side of the funnel.

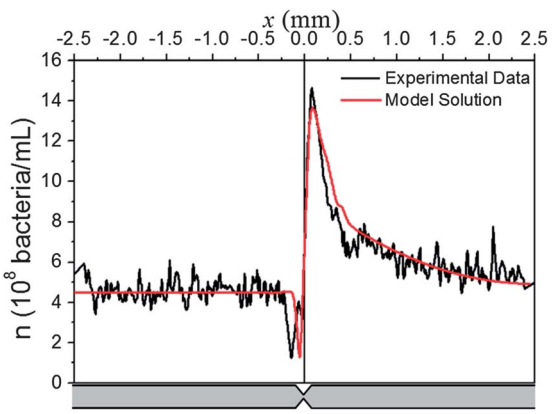

Fig. 3 Spatial extension of the symmetry breaking effect. The black line corresponds to the mean bacterial concentration measured along the flow $n(x)$. The red line is the solution of the 1-D advection–diffusion model as explained in the text. The sketch underneath corresponds to a top-view geometry of the channel at the same *X*-scale. Note the change of scale compared to the previous figures.

3 Wall absorption–desorption: the role of the funnel

To understand the mechanisms leading to this symmetry breaking and the corresponding long range density enhancement effect, we visualize and analyze the bacterial trajectories to infer qualitatively and quantitatively the salient features influencing the macroscopic transport properties of the suspension. In this part, we consider a flow velocity of $\langle V_x \rangle = 30$ μm s^{-1}, corresponding to the symmetry breaking plateau.

We start by studying the situation far away from the funnel. In Fig. 4(a), we display a snapshot of the channel far from the constriction. We superimpose on this picture, as colored lines, 30 individual bacterial trajectories (each taken over 8 s). The corresponding arrow on each line points to the forward direction of motion. This representation leads to several crucial remarks. First, we observe that a significant fraction of the trajectories are upstream (see VideoS2 in the ESI†). This upstream motion was already noticed by Hill *et al.*[24] in a straight channel of constant width. Note that there is an important number of bacteria moving upstream at the side walls which are not displayed in this figure as their trajectories are difficult to track close to the lateral boundaries. We have observed that in our confined channel bacteria can move upstream at the lateral walls over large distances. While we have no exact measure of the dwelling time of the bacteria at the lateral walls, we can estimate an upper boundary using a result obtained by Drescher *et al.*[21] who found without flow a dwelling time at the boundaries as long as 1 min. In our case, typical bacterial velocities are found to be around 15 μm s^{-1} at the lateral walls (see the spatio-temporal diagram, Fig. S2 in the ESI†) and this would lead to traveling distances at the side walls of up to 900 μm.

Second, many of the trajectories in Fig. 4(a) correspond to an "adsorption" or a "desorption" process with respect to the *lateral* left/right walls. Far from the constriction it seems that rates of adsorption and desorption are almost identical. To show this balance of desorption and adsorption, we measured directly the number of bacteria crossing a plane parallel to the side walls at a distance of 10 μm from the wall during 8 s. We deduced from these measurements that, either far before or after the funnel, the mean lateral flux $J(x) = J^+(x) - J^-(x)$ is almost zero. Note that we define $J^+(x)$ as the flux of bacteria going from the side walls (left or right) to the bulk and $J^-(x)$ as the flux of bacteria going from the bulk to the side walls. We obtained $J^+(x) \approx J^-(x) \approx 0.0028$ bact per μm^2 per s.

We also measured the bacterial density profile across the channel width on the left and on the right sides of the funnel. The profiles $n(y)$ are displayed in Fig. 4(b) and the flux equilibration is consistent with the flatness of the profile. From these profiles one can also see that there is an important bacterial population very near the lateral walls in agreement

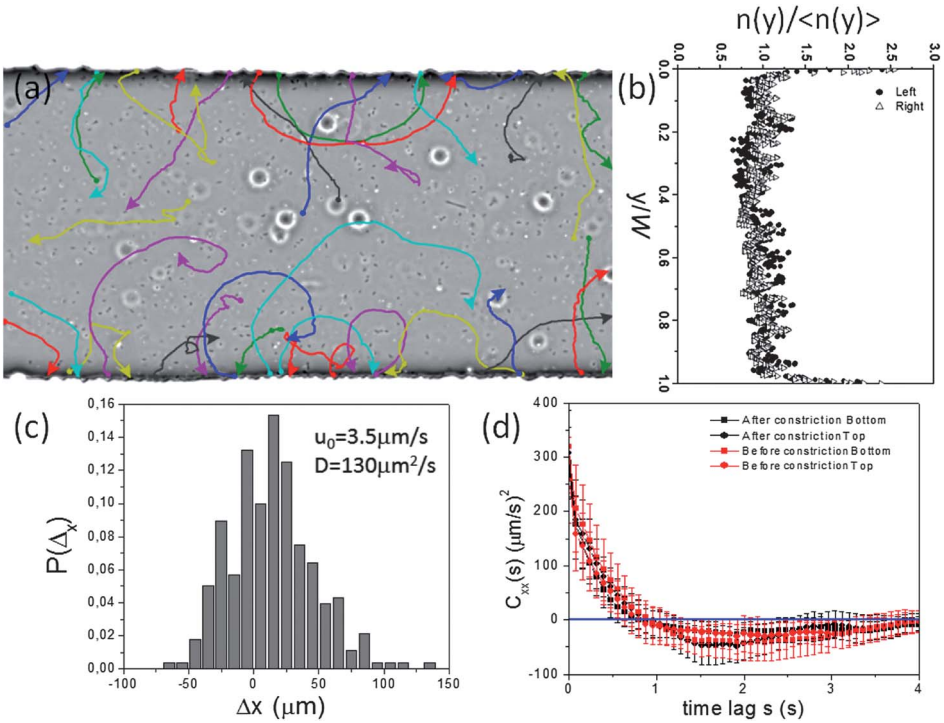

Fig. 4 (a) Bacterial trajectories superimposed to a snapshot far from the funnel ($x = 1.7$–2.1 mm), showing side wall adsorption and desorption effects. (b) Transverse bacterial concentration as a function of vertical position y. Dark circles and empty triangles represent the profile measured between -2.1 and -1.7 mm and between 1.7 and 2.1 mm, respectively. $\langle n(y)\rangle = 4.25 \times 10^8$ bact. per mL and $\langle n(y)\rangle = 5.5 \times 10^8$ bact. per mL represent the mean concentration before and after the funnel, respectively. (c) Mean displacement distribution $P(\Delta x)$. The statistics is taken over 280 trajectories. (d) Longitudinal velocity autocorrelation C_{xx} as a function of the time lag s (see text for definition).

with our observation of an important upstream traffic of bacteria in this region.

To quantify the mean transport properties due to the flow, we tracked 280 bacterial trajectories far from the funnel (on both sides) during $\tau = 4$ s. The corresponding displacements Δ_x along the flow were computed. In Fig. 4(c), the corresponding distribution $P(\Delta_x)$ is displayed. From the mean value $\overline{\delta X} = 14$ μm and the average quadratic deviation from the mean $\overline{\sigma_x^2} = 1040$ μm^2, we obtain a mean transport velocity far from the funnel $u_0 = \overline{\delta X}/\tau = 3.5$ μm s^{-1} and the corresponding dispersion coefficient along the flow $D = \overline{\sigma_x^2}/2\tau = 130$ μm^2 s^{-1}. The mean transport velocity is almost one order of magnitude smaller than the mean flow velocity. Importantly, we have checked that the time scale $\tau = 4$ s is appropriate to compute the emerging macroscopic quantities. In Fig. 4(d), we display the mean longitudinal velocity autocorrelations $C_{xx}(s)$ for a time lag s: $C_{xx}(s) = \left\langle \overline{V_x^b(t+s)V_x^b(t)} \right\rangle_b - \left\langle \overline{V_x^b(t)}^2 \right\rangle_b$. Note the double average: a time average along each track, and a second average over the 280 bacterial trajectories. The error bars correspond to the RMS deviation for the different trajectories. The "instantaneous" bacterial velocity along the track $V_x^b(t)$ was computed with a time scale resolution $\delta t = 0.08$ s. For a time lag of $s = 4$ s, the autocorrelation has reached – within experimental uncertainties – a zero value which means that computing the mean transport properties using the time scale $\tau = 4$ s is meaningful.

Thereafter, we look at the region close to the funnel. To characterize the adsorption–desorption effects at the lateral walls, we computed the average fluxes $J(x) = J^+(x) - J^-(x)$, in a region around the funnel *i.e.* for -150 μm $< x <$ 500 μm (see Fig. 5(a)). The values $J(x)$ are displayed in Fig. 5(b). Note that, as explained above, positive values mean net "desorption" and negative values mean net "adsorption". We observe a strong peak of desorption at the funnel constriction, followed by a slightly increased adsorption in

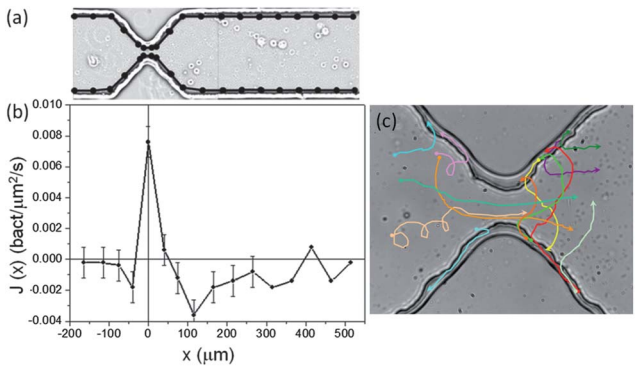

Fig. 5 (a) Snapshot of the funnel area on which are superposed the segments used to count the number of bacteria crossing in and out of the lateral walls in order to define the transverse fluxes. Each segment is of approximately 50 μm length (except in the constriction area where they are shorter). (b) Plot of the transverse flux $J(x)$ corresponding to the number of bacteria crossing the segments in/out of the walls per unit time. Note that when $J(x) > 0$, bacterial desorption dominates and when $J(x) < 0$, absorption dominates. At distances larger than 2000 μm to the right, the net flow is zero. (c) Zoom on the funnel area with 10 trajectories handtracked during 4 seconds. The mean flow is 25 μm s^{-1}.

the region downstream of the funnel. This effect persists over a large distance and the equilibrium value of $J = 0$ is not yet reached after 500 microns.

More qualitatively, the symmetry breaking in the vicinity of the constriction can be illustrated by following several typical trajectories of the bacteria. In Fig. 5(c), we display a snapshot of the funnel area and superimpose on the figure, some trajectories as in Fig. 4(a). We see that the bacteria moving upstream at the lateral walls and approaching the constriction will undergo "forced" desorption, most likely due to the increase of viscous shear stress, and will be recycled into the flow. Typical shear rates at the lateral wall at the onset of symmetry breaking are found to be around 30 s^{-1} (see previous section). The strong tendency to be detached at the funnel is responsible for the big positive peak of the mean flux $J(x)$ seen in Fig. 5(b). The higher concentration of bacteria observed at the right side of the funnel (see Fig. 3) is caused by this increased "desorption" at the funnel and might also be at the origin of increased adsorption (and thus a negative mean flux $J(x)$) along the lateral walls further down to the right side of the funnel. Increased adsorption on the lateral walls might also be due to the fact that bacteria are reoriented in the divergent flow downstream of the restriction. This scenario is in agreement with the individual bacterial trajectories displayed in Fig. 5(b): while some bacteria re-incorporate into the bulk and are just advected to the far right (where they are eventually re-absorbed by the walls), others are re-absorbed almost immediately, typically on the opposite wall. Those bacteria then undergo premature desorption at the funnel, increasing the concentration even further. We have estimated that bacteria can travel upstream at the lateral walls over distances as long as 900 μm. The equilibrium over adsorption and desorption fluxes thus takes place over distances of this order of magnitude. This length might explain why the adsorption–desorption fluxes stay unbalanced over large distances (corresponding to the wide negative curve $J(x)$) at the right of the funnel seen in Fig. 5(b). The scenario at the left of the funnel is quite different. The geometry of the funnel might facilitate bacteria moving downstream in the bulk to "hit" the walls and get attached – that process might explain the negative peak of $J(x)$ at the left side of the funnel in Fig. 5(b).

4 Anomalous dispersion

Now, to provide a quantitative picture of the influence of a funnel-like structure on the transport and the dispersion properties of a bacterial suspension, we map the problem onto a simple one dimensional advection–diffusion equation taken at steady-state:

$$-D\frac{d^2n(x)}{dx^2} + \frac{d}{dx}[u_a(x)n(x)] = S(x) \quad (2)$$

where $n(x)$ is the volume concentration of bacteria, $u_a(x)$ is their mean advection velocity along the flow, D is an effective longitudinal dispersion coefficient and $S(x)$ is a conservative bulk source/sink term coming from the lateral wall contributions. The source-sink term is defined as $S(x) = J(x)/w(x)$, where $w(x)$ is the channel width at position x. Since the total number of bacteria must be conserved, the condition $\int S(x)dx = 0$ must be fulfilled (the integration taking place along the whole channel).

To pursue the analysis quantitatively, we now assume that the mean bacterial velocity is proportional to the local flow velocity, which gives a relationship between the local advection velocity and u_0, the mean advection velocity far from the funnel: $u_a(x) = \frac{W}{w(x)}u_0$. If $S(x)$ is known, only two parameters remain to be introduced in eqn (2): u_0 and D. Provided the values computed previously from the distribution of the longitudinal displacements (see Fig. 4(c)): $u_0 = 3.5$ μm s^{-1}, $D = 130$ μm^2 s^{-1}, and the experimental values for $S(x)$ from the $J(x)$ measurement (see Fig. 5(b)), the equation can be integrated numerically with the boundary conditions at $x = -\infty$, $n(-\infty) = 4.5 \times 10^8$ bact. per mL and $dn/dx(-\infty) = 0$. The result is displayed in Fig. 3 (red curve). We observe a good agreement with the experimental determination of the density along the flow which means that we have identified the necessary parameters to describe the transport and dispersion of bacteria in this micro-channel.

5 Conclusion

We have shown experimentally that a suspension of *E. coli* passing through a micro-fluidic channel with a funnel-like constriction displays anomalous dispersion properties, which allows a control of a bacterial concentration profile just by manipulating the flow intensity or its direction.

A crucial element here is the presence of bacterial motion at the walls, which features may differ significantly in magnitude and even in direction from the mean bacterial motion in the bulk. As a consequence, the typical sojourn times can be extremely long with respect to the bulk transport time for the channel dimensions. This has direct consequences on the spatial distribution of bacteria under flow and could impact more generally our vision of bacterial transport in porous and in confined media. Due to large hydrodynamic stresses, the presence of a constriction is forcing locally the desorption of the bacteria moving at the wall and then modifies the balance of adsorption–desorption processes in the downstream direction over large distances. The phenomenon we have reported here is essentially due to the active character of the suspension and cannot be assimilated to the straining effects described when filtering colloidal suspensions. We have shown that taking into account this non-local process as a conservative bulk source term, we can reproduce without free fitting parameters the mean concentration distribution of the bacteria along the channel.

Selected additional experiments have shown that a densification is observed also for different shapes of the constriction. In the future, it seems important to quantify this densification, the sojourn time and the motion of the bacteria at the walls under flow, as a function of the geometry of the micro-fluidic channel in detail. Our results also open the possibility to control hydrodynamically the concentration and delivery of motile bacteria depending on their activity, but this will be the subject of a future report.

Acknowledgements

E.A. and G.M. have contributed equally to this work as far as data collection, analysis and final discussion are concerned and thus should share formally the first author position in the authors list. We thank H. Berthet, F. Monti and M. Hoyos for help in the microchannel fabrication, J. C. Carrillo for help on tracking and O. Ramos and I. Galperin for useful discussions. We acknowledge financial support from the Pierre-Gilles de Gennes Foundation, Sesame Ile-de-France and the ESPCI for Joliot-Curie and Total invited chairs. G.M. is particularly grateful for a special financial support from the MESR *via* the LIA-Physique et Méchanique des Fluides.

References

1 A. Baskarana and M. C. Marchetti, Statistical mechanics and hydrodynamics of bacterial suspensions, *Proc. Natl. Acad. Sci. U. S. A.*, 2009, **106**, 15567.
2 D. L. Koch and G. Subramanian, Collective hydrodynamics of swimming micro-organisms: living fluids, *Annu. Rev. Fluid Mech.*, 2011, **43**, 637–659.
3 M. F. Copeland and D. B. Weibel, Bacterial swarming: a model system for studying dynamic self-assembly, *Soft Matter*, 2009, **5**, 1174–1187.
4 X.-L. Wu and A. Libchaber, Particle diffusion in a Quasi-two-dimensional bacterial bath, *Phys. Rev. Lett.*, 2000, **84**, 3017.
5 G. Miño, T. E. Mallouk, T. Darnigue, M. Hoyos, J. Dauchet, J. Dunstan, R. Soto, Y. Wang, A. Rousselet and E. Clément, Enhanced diffusion due to active swimmers at a solid surface, *Phys. Rev. Lett.*, 2011, **106**, 048102.
6 J. Dunkel, V. B. Putz, I. M. Zaid and J. M. Yeomans, Swimmer-tracer scattering at low reynolds number, *Soft Matter*, 2010, **6**, 4268–4276.
7 A. Sokolov and I. Aranson, Reduction of viscosity in suspension of swimming bacteria, *Phys. Rev. Lett.*, 2009, **103**, 148101; D. Saintillan, The dilute rheology of swimming suspensions, *Exp. Mech.*, 2010, **50**, 1275.
8 S. Rafaï, L. Jibuti and P. Peyla, Effective viscosity of microswimmer suspensions, *Phys. Rev. Lett.*, 2010, **104**, 098102.
9 M. J. Kim and K. S. Breuer, Controlled mixing in microfluidic systems using bacterial chemotaxis, *Anal. Chem.*, 2007, **79**, 955.
10 C. Dombrowski, L. Cisneros, S. Chatkew, R. E. Goldstein and J. O. Kressler, Self-concentration and large-scale coherence in bacterial dynamics, *Phys. Rev. Lett.*, 2004, **93**, 098103.
11 A. Sokolov, *et al.*, *Proc. Natl. Acad. Sci. U. S. A.*, 2009, **107**, 969; R. Di Leonardo, *et al.*, *Proc. Natl. Acad. Sci. U. S. A.*, 2010, **107**, 9541.
12 G. M. Hornberger, A. L. Mills and J. S. Herman, Bacterial transport in porous media: evaluation of a model using laboratory observations, *Water Resour. Res.*, 1992, **28**, 915–938.
13 S. A. Bradford, J. Simunek and S. L. Walker, Transport and straining of *E. coli* O157:H7 in saturated porous media, *Water Resour. Res.*, 2006, **42**, W12S12.
14 H. C. Berg, E. coli *in Motion*, Verlag, New York, 2004.
15 N. C. Darnton, L. Turner, S. Rojevsky and H. C. Berg, On torque and tumbling in swimming *Escherichia coli*, *J. Bacteriol.*, 2007, **189**, 1756.
16 E. Korobkova, T. Emonet, J. M. G. Vilar, T. S. Shimizu and P. Cluzel, From molecular noise to behavioral variability in a single bacterium, *Nature*, 2004, **428**, 574.
17 P. D. Frymier, *et al.*, 3-Dimensional tracking of motile bacteria near a solid planar surface, *Proc. Natl. Acad. Sci. U. S. A.*, 1995, **92**, 6195.
18 E. Lauga, W. R. DiLuzio, G. M. Whitesides and H. A. Stone, Swimming in circles: motion of bacteria near solid boundaries, *Biophys. J.*, 2006, **90**, 400.
19 S. van Teeffelen, U. Zimmermann and H. Loswen, Clockwise-directional circle swimmer moves counter-clockwise in Petri dish- and ring-like confinements, *Soft Matter*, 2009, **5**, 4510–4519.
20 G. Li and J. X. Tang, Accumulation of microswimmers near a surface mediated by collision and rotational brownian motion, *Phys. Rev. Lett.*, 2009, **103**, 078101.
21 K. Drescher, J. Dunkel, L. H. Cisneros, S. Ganguly and R. E. Goldstein, Fluid dynamics and noise in bacterial cell-cell and cell-surface scattering, *Proc. Natl. Acad. Sci. U. S. A.*, 2011, **108**, 10940.
22 P. Galajda, J. Kleymer, P. Chaikin and R. Austin, A wall of funnels concentrates swimming bacteria, *J. Bacteriol.*, 2007, **189**, 8704.
23 E. Hulme, W. R. DiLuizio, S. S. Shevkoplyas, C. Turner, M. Mayer, H. C. Berg and G. M. Whitesides, Using ratchets and sorters to fractionate motile cells of *Escherichia coli* by length, *Lab Chip*, 2008, **8**, 1888.
24 J. Hill, O. Kalkanci, J. L. McMurry and H. Koser, Hydrodynamic surface interactions enable *Escherichia coli* to seek efficient routes to swim upstream, *Phys. Rev. Lett.*, 2007, **98**, 068101.
25 T. Ahmed and R. Stocker, Experimental verification of the behavioral foundation of bacterial transport parameters using microfluidics, *Biophys. J.*, 2008, **95**, 4481–4493.
26 D. Genovese and J. Sprakel, Crystallization and intermittent dynamics in constricted microfluidic flows of dense suspensions, *Soft Matter*, 2011, **7**, 3889–3896.
27 C. T. Archer, J. F. Kim, H. Jeong, J. H. Park, C. E. Vickers, S. Y. Lee and L. K. Nielsen, The genome sequence of *E. coli* W (ATCC 9637): comparative genome analysis and an improved genome-scale reconstruction of *E. coli*, *BMC Genomics*, 2011, **12**, 9.
28 B. M. Prüβ and P. Matsumura, Cell cycle regulation of flagellar genes, *J. Bacteriol.*, 1997, **179**, 5602.
29 T. Minamino, Y. Imae, F. Oosawa, Y. Kobayashi and K. Oosawa, Effect of intracellular pH on rotational speed of bacterial flagellar motors, *J. Bacteriol.*, 2003, **185**, 1190–1194.
30 F. M. White, *Viscous Fluid Flow*, McGraw-Hill, 2005.